Research Article

Huiwen Zheng, Yin Li, Wei Li, Sha Zhou, Chunlan Huang, Lizhong Du*

Ultrasound induced biosynthesis of silver nanoparticles embedded into chitosan polymers: Investigation of its anti-cutaneous squamous cell carcinoma effects

https://doi.org/10.1515/chem-2024-0018
received December 24, 2023; accepted April 2, 2024

Abstract: Here we have shown the novel biosynthesis of silver nanoparticles (Ag NPs) encapsulated by chitosan polymers in the presence of *Achillea millefolium* aqueous extract (Ag NPs@CHI). The Ag ions were first embedded over the chitosan surface enriched with polar organofunctions like amines (NH_2) and hydroxyls, and subsequently the ions were reduced green-metrically by the electron rich phytochemicals of the plant extract. After the synthesis numerous techniques, including the UV-vis spectrum, transmission electron microscopy, FE-SEM, EDS-elemental mapping, and ICP-AES, were used to study the physicochemical characteristics of the nanocomposite biomaterial. Next, we explored the material biologically in the anti-cutaneous squamous cell carcinoma effects against the corresponding cell lines like PM1, MET1, MET 4, SCC T9, SCC IC1MET, SCC IC19, SCC T8, and SCC T11. The related IC_{50} values of the nanocomposite against them were 182, 158, 177, 178, 177, 99, 62, and 183 μg/mL, respectively. The cytotoxicity in terms of percentage cell viability of cancer cells were decreased with the increase in the nanocomposite doses.

Keywords: *Achillea millefolium*, Ag nanoparticles, chitosan, cutaneous squamous cell carcinoma, cytotoxicity

1 Introduction

Now a days medical researchers are inclined to employ plant extracts to cure cancer in addition to chemical medications which have severe side effects, following the human awareness of the efficacy of medicinal plants in treating deadly diseases like cancer [1–4]. Herbal medicines, either in combination with anticancer drugs or alone, have demonstrated positive therapeutic outcomes in certain resistant cases. In contrast, modern medicine alone has proven ineffective in treating these cases [3–6]. Medicinal plants are a viable option for mitigating the disease efficacies. The medicinal plants' affordable price, lower toxicity, minimal side effects, and accessibility make them valuable alternatives to chemical drugs [6–9]. *Achillea millefolium* has been utilized for various purposes such as treating gall bladder insufficiency, reducing blood pressure, preventing kidney stones, stopping bleeding, regulating women's menstrual cycles, addressing children's enuresis, inducing relaxation, repelling Ascaris parasites, alleviating cold symptoms, treating skin acne, and relieving muscle pain [10–12]. The antidiabetic properties have been scientifically substantiated. Studies have demonstrated its efficacy in decreasing blood pressure, lowering blood cholesterol and fat levels, exhibiting antimicrobial effects, and mitigating the seizures severity [13–15].

In addition to the wide array of chemical drugs employed in carcinoma treatment, the medicinal plants integration with diminished negative impacts can function as a supplementary approach and potentially a substitute for chemical drugs. There has been a collaborative effort between the traditional and modern scientific communities to develop advanced medications for combating this fatal illness [3,6–9]. With the emergence of nanotechnology, researchers have focused on creating nanomedicines that combine traditional medicine and plant-based remedies, resulting in a diverse range of efficient compounds for carcinoma management [16].

*** Corresponding author: Lizhong Du,** Department of Neonatology, Children's Hospital Zhejiang University School of Medicine, National Clinical Research Center for Child Health, No. 3333, Binsheng Road, Binjiang District, Hangzhou, Zhejiang, 310052, China, e-mail: dulizhong@zju.edu.cn
Huiwen Zheng, Yin Li, Wei Li, Sha Zhou, Chunlan Huang: Department of Dermatology, Children's Hospital Zhejiang University School of Medicine, National Clinical Research Center for Child Health, No. 3333, Binsheng Road, Binjiang District, Hangzhou, Zhejiang, 310052, China

The nanoparticle's sustainable production has garnered notable attention owing to its several advantages as compared with the conventional methods. Furthermore, the artificial procedure is capable of being carried out under normal pressure conditions, resulting in substantial energy savings [17–21]. Various plant components, including root extract, seeds, leaves, stems, and fruit extracts, are utilized in the process as reducing agents and stabilizers [20–22]. Despite the existence of various other approaches in the NPs biosynthesis, such as the bio-macromolecules and microorganisms, as well as plant extracts, the latter option proves to be more advantageous due to its cost-effectiveness, abundance, and scalability [23,24].

Among the assortment of NPs, silver nanoparticles (Ag NPs) have indicated many therapeutic effects. This is primarily attributed to their remarkable efficacy in combating microbes, bacteria, and cancer cells, in addition to their exceptional chemical stability [25–28]. The Ag NPs use in various industries such as electronics, textiles, appliances, food and beverage, cosmetics, and healthcare has caused a notable enhance in their global consumption [29]. In addition, the green synthesis utilization for these NPs holds notable efficacy in the realm of applied pharmaceutics. Medicinal herbs have been utilized to mediate Ag NPs with green methods, which have revealed promise in curing several cancer forms [25–27]. According to recent findings, it has been discovered that the Ag NPs effectively eliminate carcinoma cells by increasing the reactive oxygen species levels within the cells [26–28]. Hence, separate research has indicated that the Ag NPs play a crucial role in permeating the membrane of carcinoma cells, ultimately leading to their demise [27,28]. The goal of this particular study is to introduce a novel method for the synthetic design and development of chitosan-capped Ag NPs, green synthesized and promoted by plant extract (Figure 1), a bioinspired procedure without using any harmful and toxic agents followed by their biological evaluation in the treatment of cancer cells. Chitosan is a unique naturally occurring carbohydrate polymer having plenteous hydroxyl groups as well as high density of amino functions, both of which provides electron rich environment that is necessary for anchoring the incoming metal ions as well as their green reduction to generate the corresponding nanoparticles. In addition, the electron rich environment also enables the NPs to stabilize by encapsulation. Also, the positively charged chitosan helps in improved ionic gelation through self-association or by different physicochemical interactions like Van der Waals, H-bonds, hydrophobic or ionic interactions, etc., which is important in determining the size of the NPs.

The green reduction is further promoted by the plenteous oxygenated phytochemicals of *A. millefolium* extract. Our devised green Ag NPs were analyzed and their cytotoxicity was clarified on a number of cutaneous squamous carcinoma cell lines like PM1, MET1, MET 4, SCC T9, SCC IC1MET, SCC IC19, SCC T8, and SCC T11 with some excellent outcomes. In literature there has not been much report on the green-mediated Ag NPs in the treatment of cutaneous squamous cell carcinoma and therefore this method itself proves its novelty.

Figure 1: *A. millefolium*'s image.

2 Experimental

2.1 Materials and methods

The catalyst preparation involved the use of chemicals such as $AgNO_3$, chitosan, [3-[4,5-dimethylthiazol-2-yl]-2,5 diphenyl tetrazolium bromide] (MTT), and various solvents, all of which were of analytical grade with a purity of over 99.5%. These chemicals were obtained from Sigma Aldrich, USA. Biochemicals like streptomycin, penicillin, glutamine, and fetal bovine serum were sourced from Fluka. The cells were purchased from Fieser, USA. The trypsin-EDTA was procured from Gibco BRL, Scotland. No further purification was required for their use. For the analytical research of the catalyst, a double beam UV–vis instrument (PG, T80+) was utilized, along with quartz cuvettes measuring 10 mm. The energy dispersive X-ray spectroscopy (EDX) studies and scanning electron microscopy (SEM) analysis were conducted using the FESEM-TESCAN MIRA3 microscope. Transmission electron microscopy (TEM) method was performed using a Zeiss microscope, operating at 300 kV.

2.2 Preparation of *A. millefolium* extract

The *A. millefolium* (1.0 g) plant (Figure 1) being washed and dried was added to 20 mL of DI water, and warmed for 0.5 h at 80°C. The plant suspension was then filtered over Whatman-1 paper and applied as intended.

2.3 Synthesis of Ag NPs

A solution of 0.1 g chitosan in 10 mL *A. millefolium* plant extract was prepared by sonication and then the Ag precursor, $AgNO_3$ aqueous solution (50 mL, 1 mM) was added to it. The mixture was again sonicated at 40°C for 0.5 h when the solution color became reddish brown, validating the generation of Ag NPs (Figure 2, inset). The prepared Ag NPs@CHI nanocomposite was collected and centrifuged for 15 min at 4,500 rpm and then rinsed with DI water.

2.4 Anticancer properties

The cytotoxic efficacies of synthesized Ag NPs@CHI nanocomposite on normal cell (HUVEC) and cutaneous squamous cell carcinoma cells (PM1, MET1, MET 4, SCC T9, SCC IC1MET, SCC IC19, SCC T8, and SCC T11) were evaluated using the MTT assay. To assess the influence of nanoparticles on cell morphology, the first stage consisted of placing 100 nanoparticles into 96-well plates. Following this, the cells were exposed to several dilations of nanoparticles every 72 h. The OLYMPUS model contrast phase microscope was employed to evaluate potential changes in cell morphology after treatment with nanoparticles, in contrast to the control group of untreated cells. The viability and growth of cells were assessed using the trypan blue dye exclusion test and a hemocytometer slide. Afterward, the cells were grown at a density of 106 cells per well. Subsequent to this, the initial plate showed no growth after a day, whereas the second plate was exposed to around 900 µg/mL of methanol as a control for the solvent. Different doses of NPs were introduced to the rest of the plates, and each

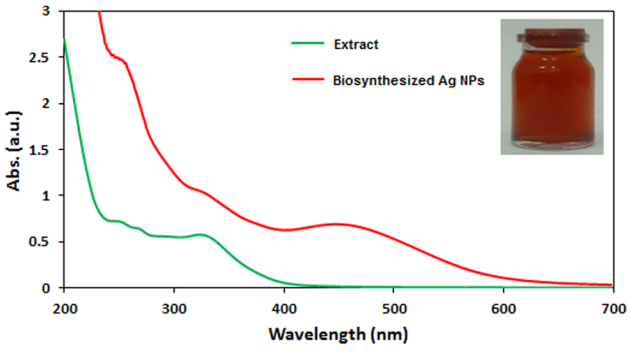

Figure 2: UV–vis analysis of the biosynthesis of Ag NPs@CHI and image of the nanocomposite solution (inset).

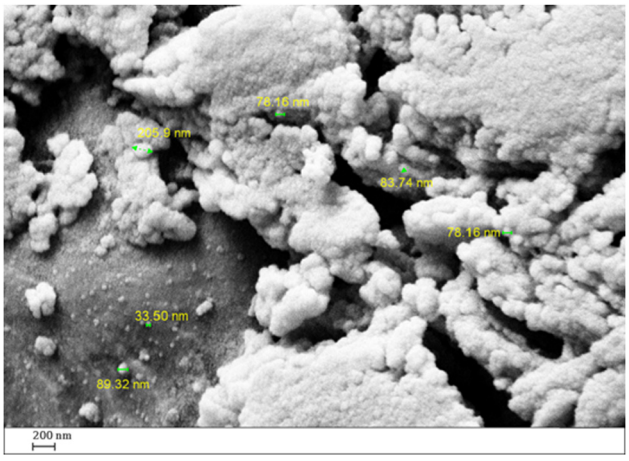

Figure 3: FE-SEM image of biosynthesized Ag NPs@CHI.

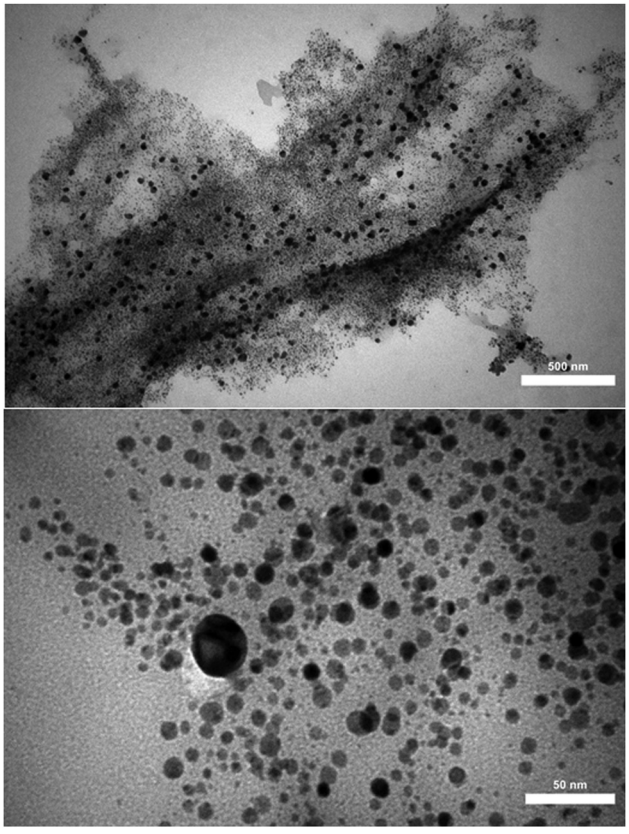

Figure 4: TEM images of Ag NPs@CHI.

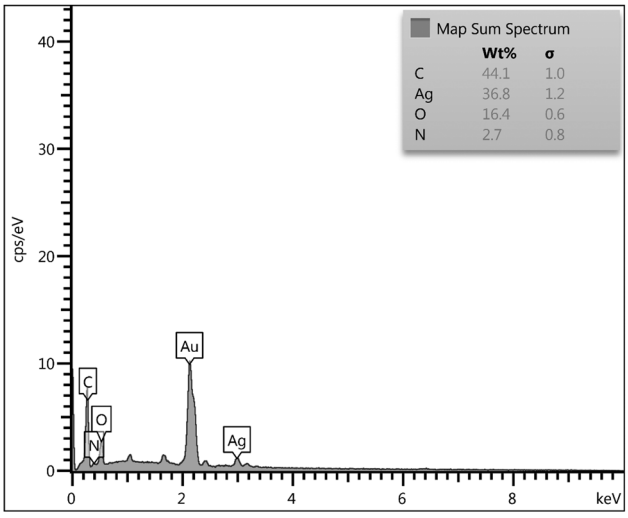

Figure 5: EDX data of biosynthesized Ag NPs@CHI.

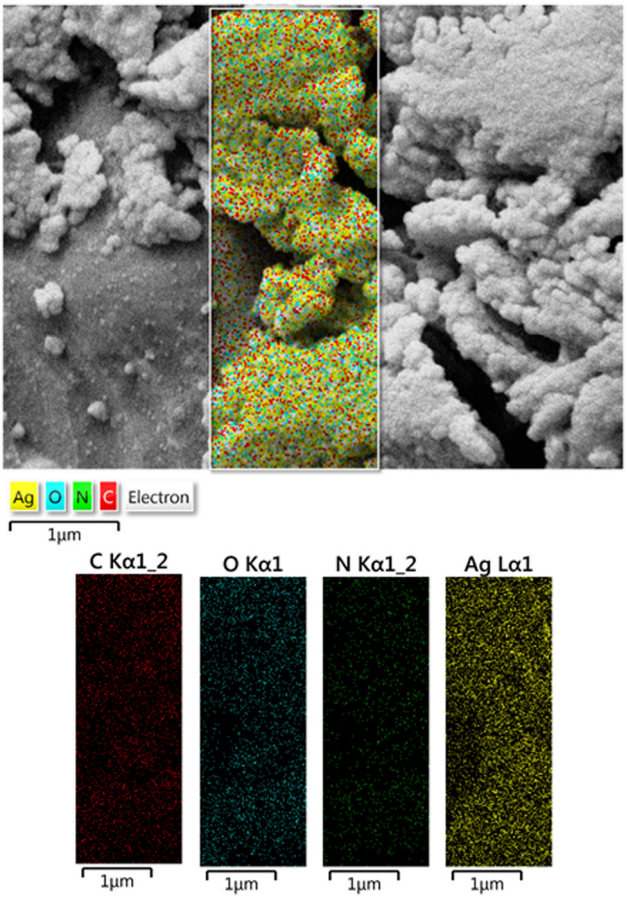

Figure 6: SEM-elemental mapping of Ag NPs@CHI.

dosage was replicated three times. The dishes were subsequently transferred to an incubator adjusted to 5% CO_2, 37°C, 90% humidity, and 95% oxygen for a duration of 24 h. Subsequently, the dishes were analyzed to determine the IC_{50} value. Throughout a span of 3 days, MTT solution quantities were added and allowed to incubate for 8 h. Afterward, the formazan crystals were dissolved in 0.1 L of dimethyl sulphoxide, and their absorption at 570 nm was quantified using a Biotech ELISA reader produced in Germany [30,31]:

$$\text{Cell viability}(\%) = \frac{\text{Sample A}}{\text{Control A}}.$$

2.5 Statistical analysis

Minitab-21 was applied to follow the normality of the data. Following this, the non-normal data were corrected. SPSS-22 was used for data variance analysis, and the visual representations were generated using Excel.

3 Results and discussion

The novel hybrid nanomaterial was prepared paved by a bio-inspired green reduction method. A hydrogel solution of *A. millefolium* extract and chitosan was used as the template to generate the Ag NPs *in situ* from its precursor salts. Following this pathway the metal ions were reduced promoted by the electron rich organo-functions contained in

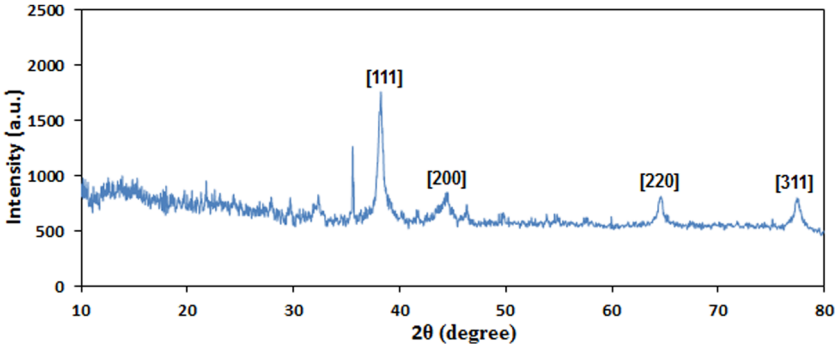

Figure 7: XRD pattern of Ag NPs@CHI.

Table 1: IC_{50} of nanocomposite in the anti-cutaneous squamous cell carcinoma test

IC_{50}	Nanocomposite (µg/mL)
PM1	182 ± 4
MET1	158 ± 6
MET4	177 ± 3
SCC T9	178 ± 4
SCC IC1MET	177 ± 5
SCC IC19	99 ± 5
SCC T8	62 ± 7
SCC T11	183 ± 5

the green tea-CS hydrogel. The organogel encapsulation additionally facilitated the electronic stabilization of Ag NPs by capping. The so formed Ag NPs@CHI nanocomposites were characterized. Synthesis of the Ag NPs@CHI can be perceived by visible observations only, while changing the solution color from yellow to light-brown, as indicated in Figure 2. The outcome was further validated by a time-dependent UV–vis spectroscopic investigation and consequently a broad hump for Ag NPs emerged at 450 nm, an interpretation of its characteristic surface plasmon resonance. The result is displayed in Figure 2, where the absorption of Ag-nanocomposite can be clearly distinguished from the *A. millefolium* extract-CS hydrogel. The unmetalled hydrogel extract displays an absorption at 335 nm which diminished gradually in the latter graph when Ag ions got reduced to its NPs over the CS-*Achillea* hydrogel and a prominent absorption was noticed at 450 nm in 30 min of reaction time.

In order to assess the morphological property of Ag NPs@CHI nanocomposite, FE-SEM and TEM investigations were carried out. Figure 3 shows the FE-SEM image of the prepared nanomaterial as spherical shaped with some aggregated particles due to manual preparation of the sample for recording the analysis.

TEM images of Ag NPs@CHI is given in Figure 4, the black dots show the Ag NPs with good distribution as spherical shaped without any aggregation and having sizes around 10–15 nm.

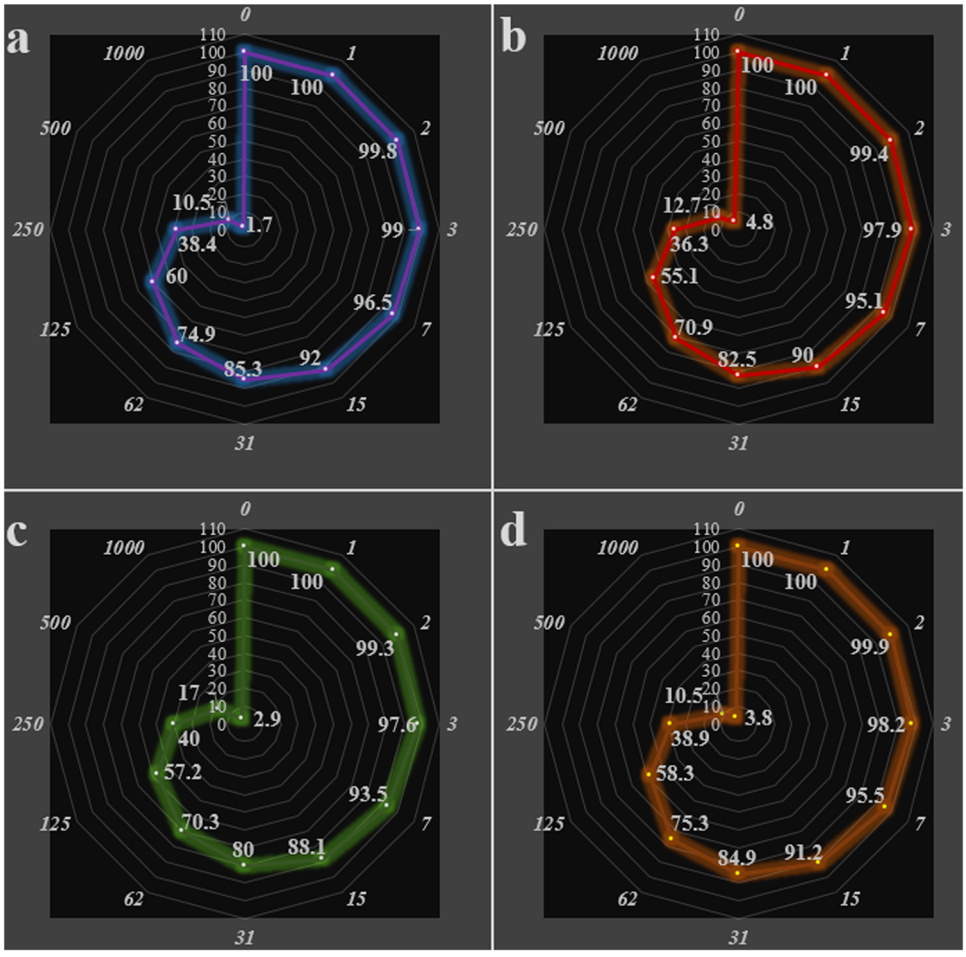

Figure 8: Anti-cutaneous squamous cell carcinoma efficacy of nanocomposite against PM1 (a), MET1 (b), MET4 (c), and SCC T9 (d) cells.

Chemical composition of the Ag NPs@CHI was estimated from EDX investigations and the corresponding outcome is presented in Figure 5. It shows Au and Ag as the metallic components and weak signals of O, N, and C at the base regions. The sharp and strong Au signal that appeared at 2.1 keV is related to the gold vapor deposition during the EDX analysis and not contributed from the original sample under investigation. The non-metals are characteristics of the *A. millefolium* phytochemicals and chitosan association within the nanocomposite sample. The corresponding map sum spectrum is also documented therein as inset which shows the atomic wt% of the elements. Markedly, Ag content in the sample is 36.8%, as compared to C content of 44.1%.

Furthermore, the elemental mapping study was done to authenticate the EDX outcome. The Ag NPs@CHI nanomaterial was subjected to SEM investigation and then X-ray scanning of a small segment, as shown in Figure 6. In the end, dispersion of the constituent elemental species is depicted as a collection of colored dots, being evenly distributed throughout the matrix. The absence of Au signals in mapping profile also justifies the discrimination from EDX result. Noticeably, applications of Ag species are greatly impacted by their homogeneity.

Finally, Ag NPs@CHI nanocomposite's crystallinity and nature of phase were confirmed by XRD analysis. The single diffraction pattern shows it as a single entity, as shown in Figure 7. The profile shows four distinct Braggs diffraction signals at 2θ = 38.2°, 44.2°, 64.3°, and 77.3°. These are accredited to the (111), (200), (220), and (311) crystal planes, respectively [32]. The diffraction range of 10–25° corresponds to a broad, non-crystalline region that represents the *Achillea*-chitosan hydrogel.

Numerous toxicological studies [33] support the common usage of Ag NPs in the profit-oriented category. Nevertheless, there is still a significant amount of knowledge to acquire regarding their impact on cells derived from mammalian tissues. Ag NPs have been found to cause cell death through various mechanisms such as autophagy, necrosis, or apoptosis. The release of Ag^{+} ions into the surrounding media

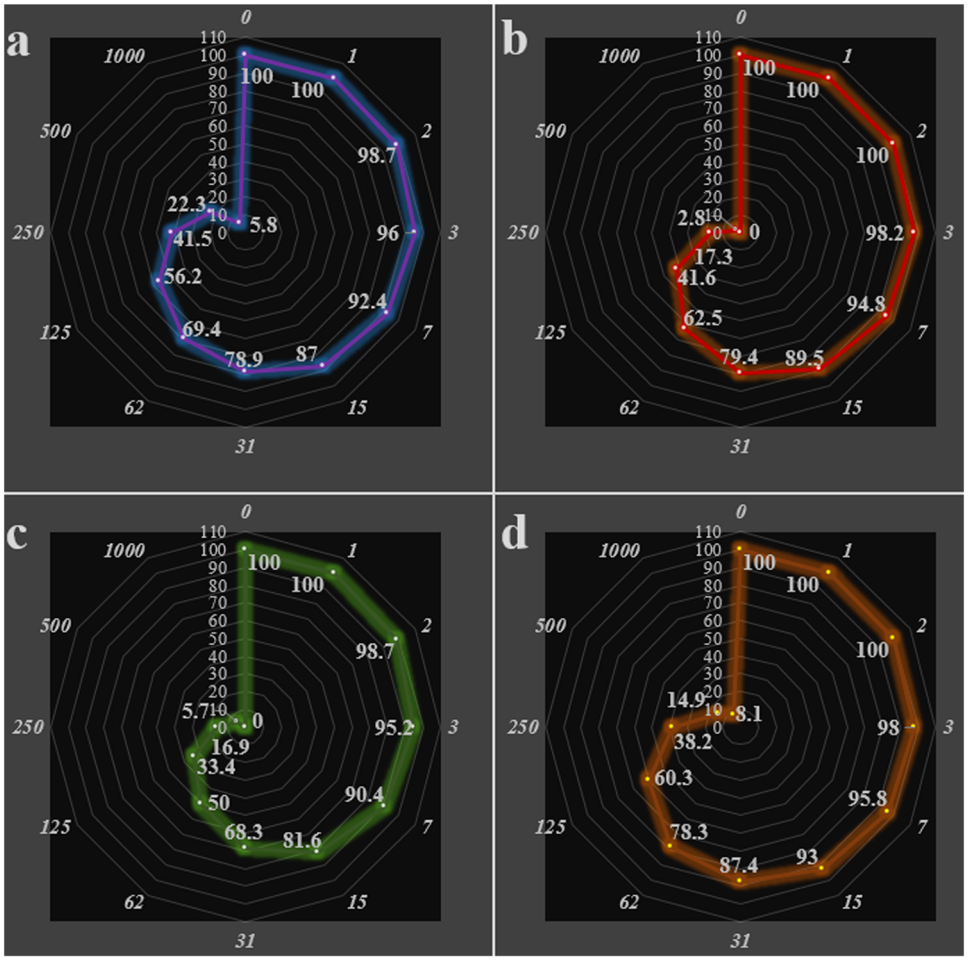

Figure 9: Anti-cutaneous squamous cell carcinoma efficacy of nanocomposite against SCC IC1MET (a), SCC IC19 (c), SCC T8 (c), and SCC T11 (d) cells.

can increase H_2O_2 amounts and initiate apoptosis [34,35]. It is crucial to emphasize that the effectiveness of Ag NPs in harming mammalian cells is influenced by several factors such as temperature duration, concentration, exposure time, shape, size, surface of nanoparticles, and the particular type of cell being examined [36–38].

In the current experiment, the cutaneous squamous cell carcinoma cells viability decreased in the Ag NPs presence. The IC_{50} of Ag NPs was 182, 158, 177, 178, 177, 99, 62, and 183 µg/mL on PM1, MET1, MET 4, SCC T9, SCC IC1MET, SCC IC19, SCC T8, and SCC T11 cells, respectively (Table 1; Figures 8, 9).

The cell viability examination plays a vital role in toxicology studies. It helps to understand the effects of various toxic substances on cells and offers valuable information on metabolic processes and cell survival [39]. Recent research has shown that the Ag NPs toxicity on HeLa cells rises as the concentration increases [40]. The enhanced toxic effect of Ag NPs on MCF7 cells is linked to decreased viability, increased apoptosis, and reduced cell growth [41]. Franco-Molina et al. discovered that colloidal Ag has a cytotoxic efficacy on breast carcinoma cells [42]. The research aligns with these results, as it is confirmed that Ag NPs cause alterations in the morphology of Hep-2 and BHK-21 cells. Upon microscopic observation, it was evident that cells exposed to Ag NPs exhibited a distinct monolayer loss. A recent study by Liao et al. reported that the cytotoxic effects of Ag NPs are influenced by factors such as dosage, exposure time, and particle size, especially for particles smaller than 10 nm [43].

4 Conclusion

Finally, herein we described an efficient technique for biogenic synthesis of Ag NPs over *A. millefolium*-chitosan hydrogel in ultrasonic conditions without the use of any toxic or hazardous substances. The unmetalled hydrogel extract displays an absorption at 335 nm which diminished gradually in the latter graph when Ag ions got reduced to its NPs over the CS-*Achillea* hydrogel and a prominent absorption was noticed at 450 nm in 30 min of reaction time. In the oncological part of the recent research, the IC_{50} of Ag NPs was 182, 158, 177, 178, 177, 99, 62, and 183 µg/mL against PM1, MET1, MET 4, SCC T9, SCC IC1MET, SCC IC19, SCC T8, and SCC T11 cell lines, respectively.

Funding information: Authors state no funding involved.

Author contributions: H. Z., L. D. – conceptualization, visualization, writing—original draft, writing—review and editing; Y. L., W. L. – methodology, formal analysis, writing—review and editing; S. Z., C. H. – resources, investigation, writing—review and editing.

Conflict of interest: Authors state no conflict of interest.

Data availability statement: The datasets generated during and/or analyzed during the current study are available from the corresponding author upon reasonable request.

References

[1] Moheghi N, Tavakkol Afshari J, Brook A. The cytotoxic effect of *Zingiber officinale* in breast cancer (MCF7) cell line. Intern Med Today. 2011;17(3):28–34.
[2] Durak I, Biri H, Devrim E, Sözen S, Avcı A. Aqueous extract of *Urtica dioica* makes significant inhibition on adenosine deaminase activity in prostate tissue from patients with prostate cancer. Cancer Biol Ther. 2004;3:855–7.
[3] Konrad L, Müller HH, Lenz C, Laubinger H, Aumüller G, Lichius JJ. Antiproliferative effect on human prostate cancer cells by a stinging nettle root (*Urtica dioica*) extract. Planta Med. 2000;66:44–7.
[4] Safarinejad MR. Urtica dioicafor treatment of benign prostatic hyperplasia: a prospective, randomized, double-blind, placebo-controlled, crossover study. J Herb Pharmacother. 2005;5(4):1–11.
[5] Aydin M, Aslaner A, Zengin A. Using urtica dioica in esophageal cancer: a report of a case. Internet J Surg. 2005;7(2):1–3. https://print.ispub.com/api/0/ispub-article/9543. Accessed February 27, 2017.
[6] Alsemari A, Alkhodairy F, Aldakan A, Al-Mohanna M, Bahoush E, Shinwari Z, et al. The selective cytotoxic anti-cancer properties and proteomic analysis of *Trigonella foenum-graecum*. BMC Complement Altern Med. 2014;14:114.
[7] Amin A, Alkaabi A, Al-Falasi S, Daoud SA. Chemopreventive activities of *Trigonella foenum graecum* (fenugreek) against breast cancer. Cell Biol Int. 2005;29:687–94.
[8] Abaza MS, Orabi KY, Al-Quattan E, Al-Attiyah RJ. Growth inhibitory and chemo-sensitization effects of naringenin, a natural flavanone purified from *Thymus vulgaris*, on human breast and colorectal cancer. Cancer Cell Int. 2015;24:15–46.
[9] Al-Menhali A, Al-Rumaihi A, Al-Mohammed H, Al-Mazrooey H, Al-Shamlan M, AlJassim M, et al. *Thymus vulgaris* (thyme) inhibits proliferation, adhesion, migration, and invasion of human colorectal cancer cells. J Med Food. 2015;18:54–9.
[10] Applequist WL, Moerman DE. Yarrow (*Achillea millefolium* L.): a neglected panacea? A review of ethnobotany, bioactivity, and biomedical research. Econ Bot. 2011;65:209–25.
[11] Kowal T, Pic S. Produktywnośćgatunku *Achillea millefolium* L, w warunkach naturalnych [Productivity of the species *Achillea millejolium* L. in natural habitats]. Acta Agrobot. 2015;32:91–100.
[12] Stojanović G, Radulović N, Hashimoto T, Palić R. In vitro antimicrobial activity of extracts of four achillea species: the composition of *Achillea clavennae* L. (Asteraceae) extract. J Ethnopharmacol. 2005;101:185–90.
[13] Benedek B, Kopp B, Melzig MF. *Achillea millefolium* L. Sl – is the anti-inflammatory activity mediated by protease inhibition? J Ethnopharmacol. 2007;113:312–7.

[14] Mahady GB, Pendland SL, Stoia A, Hamill FA, Fabricant D, Dietz BM, et al. In vitro susceptibility of *Helicobacter pylori* to botanical extracts used traditionally for the treatment of gastrointestinal disorders. Phytother Res. 2005;19:988–91.
[15] Lemmens-Gruber R, Marchart E, Rawnduzi P, Engel N, Benedek B, Kopp B. Investigation of the spasmolytic activity of the flavonoid fraction of *Achillea millefolium* sl on isolated guinea-pig ilea. Arzneimittelforschung. 2005;56:582–8.
[16] Zangeneh MM, Mohammadi G, Salmani S, Razeghi Tehrani P, Rashidi K, Zangeneh A. A comparative evaluation of nephroprotective property of *Urtica dioica* L. aqueous extract and glibenclamide in diabetic mice. Res J Pharmacogn. 2020;7(1):31–40.
[17] Nie C, Du P, Zhao H, Xie H, Li Y, Yao L, et al. Ag@TiO_2 nanoprisms with highly efficient near-infrared photothermal conversion for melanoma therapy. Chem Asian J. 2020;15:148–55.
[18] Shanmugasundaram T, Radhakrishnan M, Gopikrishnan V, Kadirvelu K, Balagurunathan R. Biocompatible silver, gold and silver/gold alloy nanoparticles for enhanced cancer therapy: in vitro and in vivo perspectives. Nanoscale. 2017;9:16773–90.
[19] Swanner J, Sears JJ, Singh R, Hooker A, Donati GL, Furdui CM, et al. Silver nanoparticles selectively treat triple-negative breast cancer cells without affecting non-malignant breast epithelial cells in vitro and in vivo. FASEB BioAdv. 2019;1:639–60.
[20] Espinosa A, Curcio A, Cabana S, Radtke G, Bugnet M, Kolosnjaj-Tabi J, et al. Intracellular biodegradation of Ag nanoparticles, storage in ferritin, and protection by a Au shell for enhanced photothermal therapy. ACS Nano. 2018;12:6523–35.
[21] Hembram KC, Chatterjee S, Sethy C, Nayak D, Pradhan R, Molla S, et al. Comparative and mechanistic study on the anticancer activity of quinacrine-based silver and gold hybrid nanoparticles in head and neck cancer. Mol Pharm. 2019;16:3011–23.
[22] Liu E, Zhang M, Cui H, Gong J, Huang Y, Wang J, et al. Tat-functionalized Ag-Fe_3O_4 nano-composites as tissue-penetrating vehicles for tumor magnetic targeting and drug delivery. Acta Pharm Sin B. 2018;8:956–68.
[23] Mohseni MS, Khalilzadeh MA, Mohseni M, Hargalani FZ, Getso MI, Raissi V, et al. Green synthesis of Ag nanoparticles from pomegranate seeds extract and synthesis of Ag-starch nanocomposite and characterization of mechanical properties of the films. Biocatal Agric Biotechnol. 2020;25:101569.
[24] Khalilzadeh MA, Borzoo M. Green synthesis of silver nanoparticles using onion extract and their application for the preparation of a modified electrode for determination of ascorbic acid. J Food Drug Anal. 2016;24(4):796–803.
[25] Tang Y, Liang J, Wu A, Chen Y, Zhao P, Lin T, et al. Co-delivery of trichosanthin and albendazole by nano-self-assembly for overcoming tumor multidrug-resistance and metastasis. ACS Appl Mater Interfaces. 2017;9:26648–64.
[26] Habiba K, Aziz K, Sanders K, Santiago CM, Mahadevan LSK, Makarov V, et al. Enhancing colorectal cancer radiation therapy efficacy using silver nanoprisms decorated with graphene as radiosensitizers. Sci Rep. 2019;9:1–9.
[27] Chakraborty B, Pal R, Ali M, Singh LM, Rahman DS, Ghosh SK, et al. Immunomodulatory properties of silver nanoparticles contribute to anticancer strategy for murine fibrosarcoma. Cell Mol Immunol. 2016;13:191–205.
[28] Behnam MA, Emami F, Sobhani Z, Koohi-Hosseinabadi O, Dehghanian AR, Zebarjad SM, et al. Novel combination of silver nanoparticles and carbon nanotubes for plasmonic photo thermal therapy in melanoma cancer model. Adv Pharm Bull. 2018;8:49–55.
[29] Syafiuddin A, Salmiati, Salim MR, Kueh ABH, Hadibarata T, Nur H. A review of silver nanoparticles: research trends, global consumption, synthesis, properties, and future challenges. J Chin Chem Soc. 2017;64(7):732–56. doi: 10.1002/jccs.201700067.
[30] Lu Y, Wan X, Li L, Sun P, Liu G. Synthesis of a reusable composite of graphene and silver nanoparticles for catalytic reduction of 4-nitrophenol and performance as anti-colorectal carcinoma. J Mater Res Technol. 2021;12:1832–43.
[31] Cai Y, Karmakar B, Salem MA, Alzahrani AY, Bani-Fwaz MZ, Oyouni AAA, et al. Ag NPs supported chitosan-agarose modified Fe_3O_4 nanocomposite catalyzed synthesis of indazolo[2,1-*b*]phthalazines and anticancer studies against liver and lung cancer cells. Int J Biol Macromol. 2022;208:20–8.
[32] Yan J, Karmakar B, Zaki MSA, Osman R, Abdalla AM, Shati AA, et al. Introducing a bionanocomposite (ultrasound-assisted synthesis of Ag nanoparticles embedded aloe vera gel) for the treatment of cervical carcinoma. J Exp Nanosci. 2022;17:617–30.
[33] Tortella GR, Rubilar O, Durán N, Diez MC, Martínez M, Parada J, et al. Silver nanoparticles: toxicity in model organisms as an overview of its hazard for human health and the environment. J Hazard Mater. 2020;390:121974.
[34] Paciorek P, Żuberek M, Grzelak A. Products of lipid peroxidation as a factor in the toxic effect of silver nanoparticles. Materials. 2020; 13:2460.
[35] Rohde MM, Snyder CM, Sloop J, Solst SR, Donati GL, Spitz DR, et al. The mechanism of cell death induced by silver nanoparticles is distinct from silver cations. Part Fibre Toxicol. 2021;18:37.
[36] Gliga AR, Skoglund S, Odnevall Wallinder I, Fadeel B, Karlsson HL. Size-dependent cytotoxicity of silver nanoparticles in human lung cells: the role of cellular uptake, agglomeration and Ag release. Part Fibre Toxicol. 2014;11:11.
[37] Zhang T, Wang L, Chen Q, Chen C. Cytotoxic potential of silver nanoparticles. Yonsei Med J. 2014;55:283–91.
[38] McShan D, Ray PC, Yu H. Molecular toxicity mechanism of nanosilver. J Food Drug Anal. 2014;22:116–27.
[39] Datkhile KD, Durgawale PP, Patil MN. Biogenic silver nanoparticles are equally cytotoxic so as chemically synthesized silver nanoparticles. Biomed Pharmacol J. 2017;10(1):337–44.
[40] Jeyaraj M, Rajesh M, Arun R, Mubarak Ali D, Sathishkumar G, Sivanandhan G, An investigation on the cytotoxicity and caspase-mediated apoptotic effect of biologically synthesized silver nanoparticles using *Podophyllum hexandrum* on human cervical carcinoma cells. Colloids Surf B: Biointerfaces. 2013;102:708–17.
[41] Abrahamse H, Abdel Harith M, Hussein A, Tynga I. Photodynamic ability of silver nanoparticles in inducing cytotoxic effects in breast and lung cancer cell lines. Int J Nanomed. 2014;9(1):3771.
[42] Franco-Molina MA, Mendoza-Gamboa E, Sierra-Rivera CA, Gómez-Flores RA, Zapata-Benavides P, Castillo-Tello P, et al. Antitumor activity of colloidal silver on MCF-7 human breast cancer cells. J Exp Clin Cancer Res. 2010;29(1):148.
[43] Liao C, Li Y, Tjong SC. Bactericidal and cytotoxic properties of silver nanoparticles. Int J Mol Sci. 2019;20(2):449.